LAWRENCE
LIVERMORE
NATIONAL
LABORATORY

LLNL-TR-826595

Yield and PDV Measurements of the Godiva-IV Critical Assembly

L. A. Snyder, D. Bower, D. Fittinghoff, M. May, J. Goda, M. Pena, R. Buckles, J. Scorby

September 10, 2021

Disclaimer

This work performed under the auspices of the U.S. Department of Energy by Lawrence Livermore National Laboratory under Contract DE-AC52-07NA27344.

Lawrence Livermore National Laboratory

Preliminary Report: Yield and PDV Measurements of the Godiva-IV Critical Assembly

Lucas Snyder
Dan Bower
Robert Buckles
David Fittinghoff
Joetta Goda
Mark May
Michael Peña
John Scorby

September 27, 2021

LLNL-TR-826595

Lawrence Livermore National Laboratory is operated by Lawrence Livermore National Security, LLC, for the U.S. Department of Energy, National Nuclear Security Administration under Contract DE-AC52-07NA2734

Executive Summary

A high dynamic range, scinillator based detector, the MHD-240, was used to measure the gamma and neutron flux of several prompt critical bursts of the Godiva-IV assembly. The measurements provided the alpha and FWHM for several different burst temperatures. Calibrations of the MHD-240 gamma and neutron sensitivity along with MCNP based simulation of the Godiva-IV assembly allowed us to also determine the total fission yield of the burst integrated over approximately 5 ms.

In addition a Photo Doppler Velocimetry measurement was conducted to determine the surface motion vibrational frequency of Godiva-IV assembly during the bursts. The combined data were collected to be used as input to multi-physics simulation of the Godiva-IV assembly.

This is a preliminary report, there is an ongoing effort to update the MCNP simulations used in the analysis and develop a correction for the room return component of the measured signal.

Contents

1 Introduction

The purpose of this experiment was to collect data for a dynamic benchmark of the Godiva-IV burst assembly [1]. Data were taken using two different measurement systems. The gamma & neutron flux was measured using a calibrated, high-dynamic-range scintillator detector, the MHD-240. The measurement was used to determine the total fission yield and alpha throughout the burst and shutdown sequence of Godiva-IV. The Photon Doppler Velocimetry (PDV) measurement detected the surface motion of the burst assembly as a function of time. The combined data will be used in a multi-physics simulation of the Godiva-IV burst assembly.

Data were collected during two modes of Godiva-IV operations. First a series of four prompt critical bursts were measured with data collected on both the MHD-240 and the PDV. The MHD-240 was used to record the gamma & neutron output of Godiva over 8 orders of magnitude, which was used to infer the alpha from each burst. PDV data was successfully collected on two of the four bursts, the vibration frequency is reported. Secondly, a series of delayed critical (DC) operations were conducted with data collected on the MHD-240 to determine the room-return component of the measured neutron and gamma flux for analysis of the prompt critical bursts. Prior to the Godiva measurements the MHD-240 was calibrated separately for gamma and neutron response. The calibrations, in combination with input from an MCNP simulation and the DC measurements, will be used to determine the total fission yield.

We present herein the experimental setup, the acquired data, and analysis of the results. This was the first successful attempt to collect PDV data on the Godiva-IV (henceforth Godiva) assembly.

2 Experimental Setup

The general layout of the experiment is shown in figure 1. The PDV probes were located 1 m from Godiva. The probes were mounted using ThorLabs RC02APC-P01 Reflector collimators and KM05 kinematic mirror mounts. The probe assemblies were mounted behind lead shielding, with a line-of-sight left open for the lasers. Probes were aligned with four of the six Godiva rings, with data resolvable on only two of the rings. Figure 2 shows a schematic of the Godiva assembly and the location of the PDV probes.

The MHD-240 detector consists of a 6" cube of BC-404 scintillator with three PMTs and a photo diode (PD) arranged around four sides. Each of the four detectors are adjusted to cover a wide range of sensitivities, with about a factor of 100 separating each channel. A picture of the detector head is shown in figure 3. The signal for each of the channels was attenuated and split to two recorders. The attenuation is selected such that we can maximize use of the scopes full range for the expected signal strength. For the split signals additional attenuation was applied to the second line so that the scope sensitivity could be increased and the resolution of the measurement of the lower portion of the rising edge of the prompt critical bursts could be improved.

The gamma calibration was performed by the Mission Support and Test Services (MSTS) at NNSS using the 1.17 MeV and 1.32 MeV γ-rays from a ^{60}Co source, MSTS source designation: RAA27208 (131). The calibration results are shonw in Appendix C. The neutron calibration of the MHD-240 was conducted at Ohio University's Edwards Accelerator Laboratory [2] and is detailed in reference [3].

The DC measurements were conducted to provide data for a room-return correction of the prompt critical analysis. The MHD-240 was located at distances of both 2 and 4 m with and without shielding. The shielded and un-shielded measurements provided data on the relative

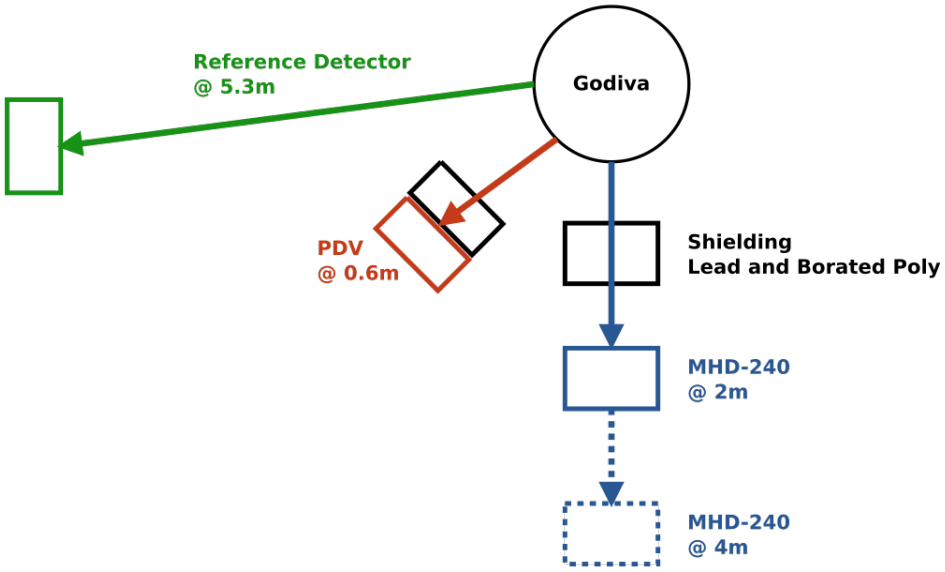

Figure 1: The layout of the detectors relative to the Godiva assembly. The MHD-240 was located at 2 or 4 m, with and without shielding for the DC measurements, while the burst measurements were conducted with the MHD-240 located at 2 m with no shielding. The PDV was located 1 m from Godiva and a linear reference detector (compensated ionization chamber) was fixed at 5.3 m distance.

intensity at the detector with and without direct radiation from Godiva to determine the room-return component of the total flux. The shielding consisted of a matrix of alternating 1" thick by 12" square plates of borated polyethylene and lead with a total of 6" of each. The shielding was intended to block both the gamma and neutron component of the radiation from Godiva and was sized so as to completely shadow the MHD-240 scintillator. The shielding and the MHD-240 were elevated to the same horizontal plane as the Godiva assembly, approximately 6' from the floor. The prompt critical bursts were measured with the MHD-240 located at 2 m with no shielding in place. A picture of the overall setup is shown in figure 4.

Two detectors were deployed at a fixed position and used as reference monitors for the reactivity of various Godiva bursts. The first reference detector, termed MHD-241, has the same scintillator as the MHD-240 but with a single PMT variant with twice the photocathode area as those on the MHD-240. The second reference detector, termed LC1, is a nitrogen-helium filled proportional ion chambers, model number WL-23084 by Imaging and Sensing Technology.

A schematic the signal recording system is shown in Appendix A. The split between the high an low attenuation were on a single 8 channel LeCroy HDO8108A oscilloscope. The attenuation settings and calculations are shown in Appendix B.

3 PDV Results

PDV data was collected on two burst temperatures of 123°C and 201°C on the top and bottom of the six rings of the Godiva assembly (see figure 2). Figure 5 shows an example of one of the data sets from the bottom ring of the 201°C burst. Points are extracted from the raw data and then fit to determine the vibration frequency using custom analysis software [4]. Table 1 shows the results of all four measurements. Some general conclusions are that the top ring is consistently at a lower frequency than the bottom ring and the lower burst temperature has an overall higher

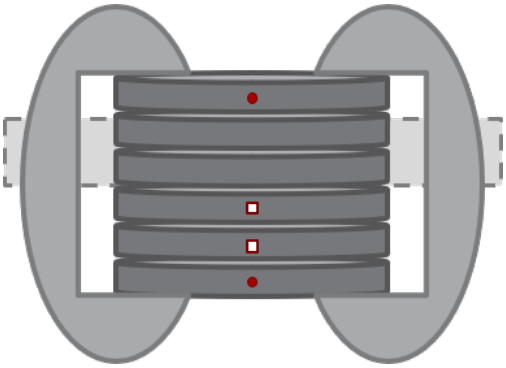

Figure 2: A schematic of the Godiva rings and clamps. The red dots indicate the location of the PDV probes, on the top and bottom rings, for which resolvable data was successfully measured. The white squares also had probes, but the data was not resolvable.

frequency. While intuition might suggest the higher temperature would have more energy and therefore a higher frequency, the bulk material properties are what dictate the frequency so this simple assumption does not necessarily hold. Any further conclusions from this data will be part of the multi-phyiscs simulation that is planned to be conducted, which is however beyond the scope of this report.

Table 1: The vibration frequency of each of the two rings for each of the two bursts. The measured frequency and the 95% confidence band are reported.

Temp. °C	Ring	Freq. (Hz)	95% Conf. (Hz)
123	Bottom	7881	7856-7907
123	Top	7729	7761-7742
201	Bottom	7545	7524-7566
201	Top	7317	7261-7327

4 MHD-240 Data Analysis Procedures and Results

4.1 Delayed Critical

The delayed critical data was collected to determine a room return correction for the prompt critical analysis. Five series of delayed critical data were collected. Two series of data at various power levels were collected with the MHD-240 located at 4 m, one with shielding and one without. Similarly, two series of data were collected with the MHD-240 at 2 m, again one with and one without shielding. The shielded and un-shielded data are analyzed relative to one-another to determine the room-return component of the total flux, whereby the shielding is intended to block the direct radiation flux from Godiva to the MHD-240. Data were collected at 2 m and 4 m to determine if there was any radial dependence to the room-return. The two reference detectors were found to be very consistent, having good linearity over all levels of power, providing a reference for the absolute flux. During the fifth series, the plastic scintillator was removed from the MHD-241 reference detector to measure any potential response from the PMT and output cabling.

Figure 6 shows the output current measured on Ch. 2 & 3 of the MHD-240, the MHD-241 (Ref. 1) and the LC1 (Ref. 2) as the reactor is stepped up through several power levels. Ref. 2 is scaled by a factor of 60 to match Ref. 1 on the plot. The fact that the scaling factor is consistent over several

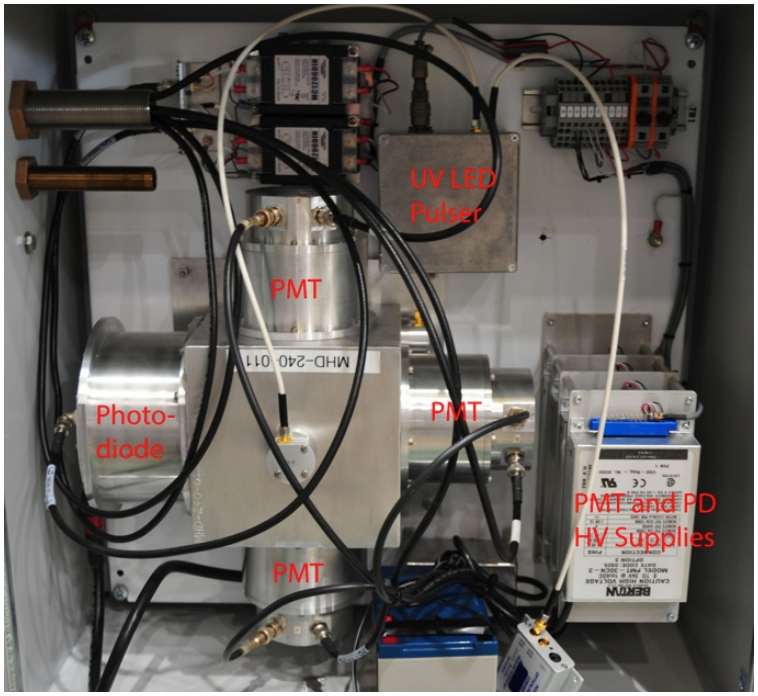

Figure 3: The MHD-240 detector head. The 3 PMTs and the photo diode are arranged on 4 sides of the 6″ cubic BC-404 scintillator.

orders of magnitude emphasizes that the two detector systems are very linear. Also shown in the figure is the scaling ratios between Ref. 1 and the MHD-240 channels. The dashes lines represent the dark level subtractions.

The general conclusion from the preliminary DC analysis is that the flux decreases for shielded measurements but are higher than they would be for a central source assuming no room return as indicated by table 2. This indicates that room return is substantial, which is to be expected for the Godiva configuration in a relatively small room with massive floor and walls. Furthermore, the supposition of $1/r^2$ for the 2 m and 4 m data sets does not hold, indicating a component of room-return from the opposite wall and/or the floor & ceiling, which is again to be expected. These data will provide a room return correction for the burst data analysis and a validation of MCNP simulations.

Table 2: Ratio of the measured current on two of the MHD-240 channels relative to the reference detector. While the ratio drops as expected for shielded measurements, the relative flux is considerably higher that would be expected for an ideal shielded point source.

	Unshielded-4m	Shielded-4m	Unshielded-2m	Shielded-2m
MHD-ch2/Ref1	1.099	0.743	2.092	0.895
MHD-ch2/Ref1	0.458	0.377	0.685	0.423

4.2 Prompt Critical

Data was successfully collected on four prompt critical bursts of the Godiva assembly at various temperatures as measured by the Godiva instrumentation (see table 4). Four channels were recorded on the MHD-240 and the detector was placed at 2 m from the assembly with no shielding

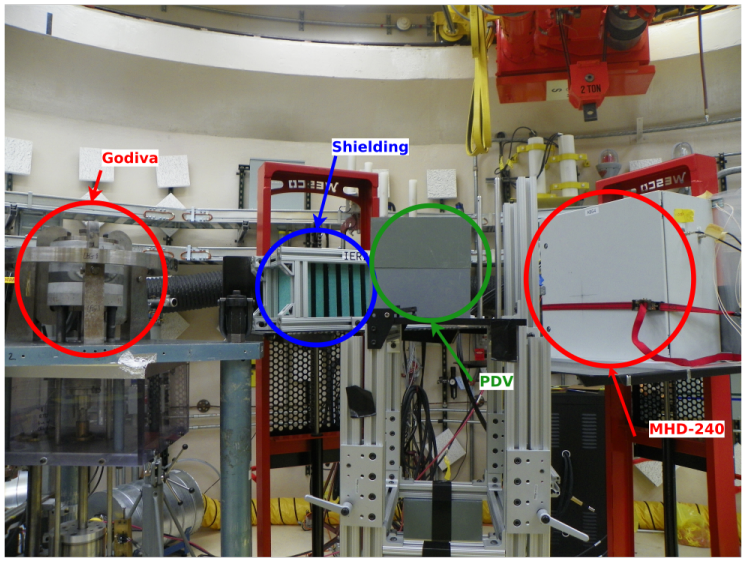

Figure 4: The Godiva-IV, shielding assembly, PDB probe assembly and MHD-240 detector can all be seen.

in place.

As was discussed in section 2 the MHD-240 consists of three PMTs and one PD arranged around four sides of a cube of scintillator (see fig. 3). The sensitivity of the four channels is adjusted such that the detector can cover many orders of magnitude, with ch. 1-4 ranging from most to least sensitive. The scope settings and attenuation are adjusted in an attempt capture the entire portion of the rising edge of the signal, before saturation, with the highest level of sensitivity on the scope that will accommodate the entire signal. The attenuator values are reported in Appendix B.

The recorded voltage is converted to a current using the measured impedance values of the scope and attenuators. These impedance values were measured and reported in Appendix B. The current can than be converted to a fission rate using the Co-60 and neutron calibrations and input from MCNP. The measured current is assumed to be the sum of the current induced by the gammas and neutrons emitted from the Godiva assembly,

$$I_{MHD} = I_\gamma + I_n \, . \tag{1}$$

The current is equal to the sensitivity of the particular channel times the rate of energy deposition,

$$I_\gamma = S_\gamma \cdot R_{E_\gamma} \, , \tag{2}$$

where S_γ is the sensitivity in units of $C/\gamma\text{-}MeV$ and the $R_{E\gamma}$ is $\gamma\text{-}MeV/s$. It is assumed that rate of energy deposition R_{E_γ} is equal to the *average* gamma energy times the rate of emission from Godiva,

$$R_{E\gamma} = \bar{E}_\gamma \cdot n_\gamma \, , \tag{3}$$

where the rate of emission is then defined number of leakage gammas times the fission rate,

$$n_\gamma = L_\gamma \cdot n_f \, . \tag{4}$$

The term "leakage gammas" is defined as the average number of gamma rays per fission event that escape from the surface of Godiva and would be available for detection. An MCNP model of

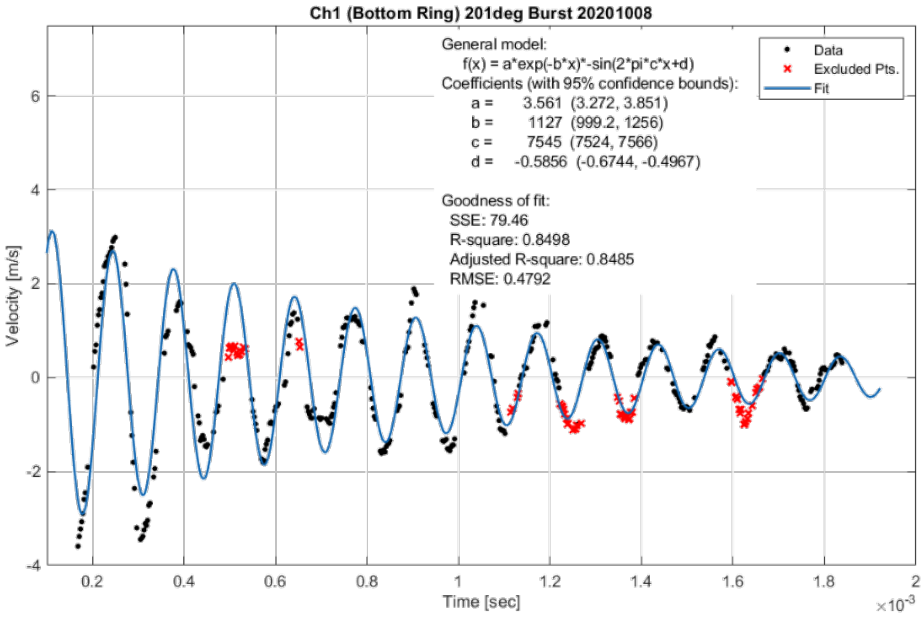

Figure 5: Data collected on the bottom ring of Godiva during the 201°C burst. Data points are extracted from the raw data and then fit to determine the vibration frequency. The fit function and various fit parameters are listed in the legend.

Godiva is used to determine $\bar{E}_\gamma$ and L_γ. The same definition can be applied to the neutrons such that the detector current can now be defined as

$$I_{MHD} = I_\gamma + I_n = n_f \cdot \bar{E}_\gamma \cdot L_\gamma \cdot S_\gamma + n_f \cdot \bar{E}_n \cdot L_n \cdot S_n \,. \tag{5}$$

Equation 5 can than be rearranged to determine the fission rate from the measured current with input from the detector calibrations and the MCNP model,

$$n_f = \frac{I_{MHD}}{\bar{E}_\gamma \cdot L_\gamma \cdot S_\gamma + \bar{E}_n \cdot L_n \cdot S_n} \,. \tag{6}$$

In the current analysis presented here estimates for the average mean leakage neutron energy E_n, was taken from ref. [5] to be approximately 2 MeV. The mean energy of the leakage gammas E_γ, was taken from ref. [6] which is also about 2 MeV. The values for number of leakage neutrons and gammas per fission L_n and L_γ, were taken from ref. [6] to be 1.57 and 0.42 respectively. The gamma sensitivity S_γ was taken from the Co-60 calibration which are reported in Appendix C. The neutron sensitivity S_n was taken from ref. [3]. The neutron calibration was only for the most sensitive channel (ch. 1). It was assumed that the neutron sensitivity for the other channels would scale like the gamma sensitivity.

The data for one of the prompt critical bursts is shown in fig. 7 where the vertical scale is adjusted based on Eq. 7. This analysis indicates that the expected relative scaling factors for the four channels is not as expected, as indicated by the red-dashed line, which is an exponential fit to the least sensitive channel (ch. 4). The line does not intersect the data from the three other channels. The signals are all recorded on the same scope with a shared time-base, therefore the horizontal alignment is not the cause of the discrepancy but rather the intensity calibration.

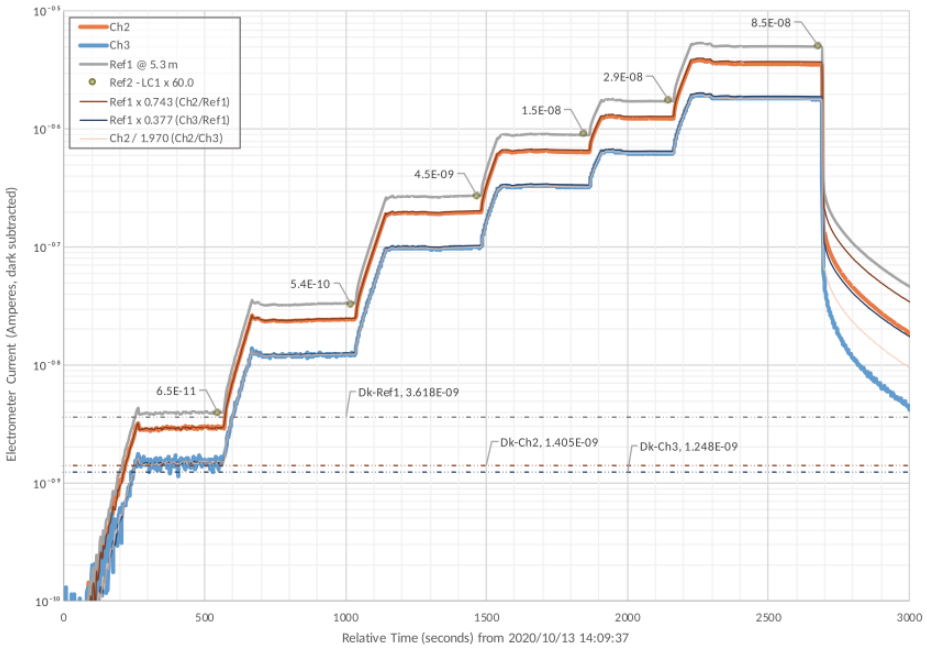

Figure 6: Delayed critical data un-shielded at 2 m. The detector current levels are shown for Ch. 2 & 3 of the MHD-240, the MHD-241 (Ref. 1) and LC1 (Ref. 2). Ref. 2 is scaled by a factor of 60 to match Ref. 1. The dashed lines represent the dark level subtractions

Ch. 4, which is equipped with the PD and is operated such that the detector will not saturate at peak reactivity. The other channels are adjusted such that at some point during the recording they are expected to saturate, at which point they will behave in a nonlinear fashion. This saturation is a result charge depletion in the PMT capacitor/resistor bridge. So while it is expected that portions of the data will not align with ch. 4, at least some region of each channel's data should overlap. This misalignment implies that additional scaling is required.

For the analysis presented here, it is assumed that the ch. 4 scaling is accurate and that the three more sensitive PMT channels will have a similar logarithmic slope or alpha, over the linear region of their response, and can be scaled overall to match ch. 4. While there are several possible causes of the scaling discrepancy between the four channels, it is likely a result of the sensitivity of the scintillator and/or optical filter changing since the calibration was performed several years ago. This change in sensitivity, or aging, has been observed in other MHD-240 detector systems. Ch. 4 does not have an optical filter, therefore it was assumed to suffer less from the potential cause of the discrepancy and chosen as the scaling baseline.

A fit search was performed over ch. 1-3 to find the region with the alpha that best matched that of ch. 4 and over which the data had a linear response, i.e. a good fit to an exponential. The data was then scaled in amplitude by the ratio of the fit constant parameter to the fit constant parameter of ch. 4. The result of one of the prompt critical data sets with the additional scaling is shown in fig. 8. The dashed lines shown in fig. 8 are the fit results and also shown is the full-width-half-max (FWHM) of the peak reactivity.

The fit search procedure involved first identifying a region of interest (ROI). The upper bound of the ROI was identified by eye where saturation becomes obvious, which is the point at where the recorded signal begins to fall and becomes erratic. To identify the lower bound we first calculate the average baseline prior to signal rise. The RMS of the noise around the baseline is then

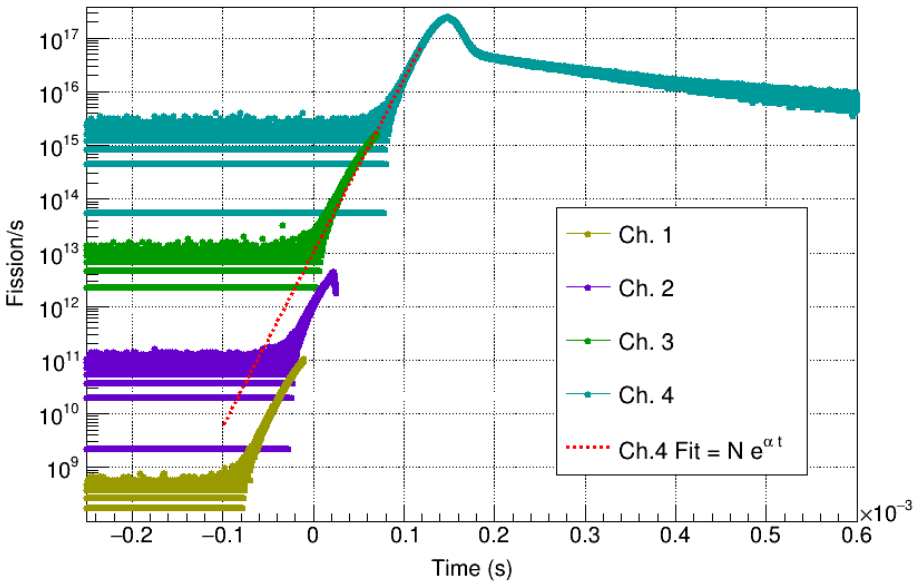

Figure 7: Data for the 201 °C burst. The red dashed line is an exponetial fit to ch. 4. The other channels are not well aligned with the fit, indicating a discrepancy in the calibration and the need for additional scaling.

calculated. A smoothing algorithm is then applied to the data, the point at which the smoothed data is greater than 2 standard deviations of the noise is selected as the lower bound. The ROI is then subdivided into 5 smaller regions and each region and every combination of neighboring regions is fit with an exponential. The fit that produces an alpha closest to that of ch. 4 is selected to determine the scaling factor. The alpha of ch. 4 was also determined with an exponential fit. Fig. 9 shows the example of ch. 1 with the results of the smoothing algorithm overlaid, also shown is the selected fit region. The scaling factors determined based on the fit search procedure are shown in table 3.

Table 3: The scaling factors for ch. 1-3 to align them with ch. 4.

Temp. °C	Ch. 1	Ch. 2	Ch. 3
70	13.78	7.02	0.34
123	34.10	8.20	2.09
168	12.04	5.50	0.47
201	33.99	0.94	0.77

As discussed previously in this section there are several possible causes for the discrepancy in the expected sensitivity of the MHD-240 channels, there are currently plans to verify the calibrations to definitively resolve this question. The effects of asymmetric room return and down-scattering of the neutrons are also still being explored. The scaling discrepancy has no effect on the determination of alpha or the FWHM presented here. The alpha and FWHM for each prompt critical burst are listed in table 4. Further analysis however will be needed to resolve the overall scaling factors.

The fission yield for the current scaling analysis, with no room return correction, is presented

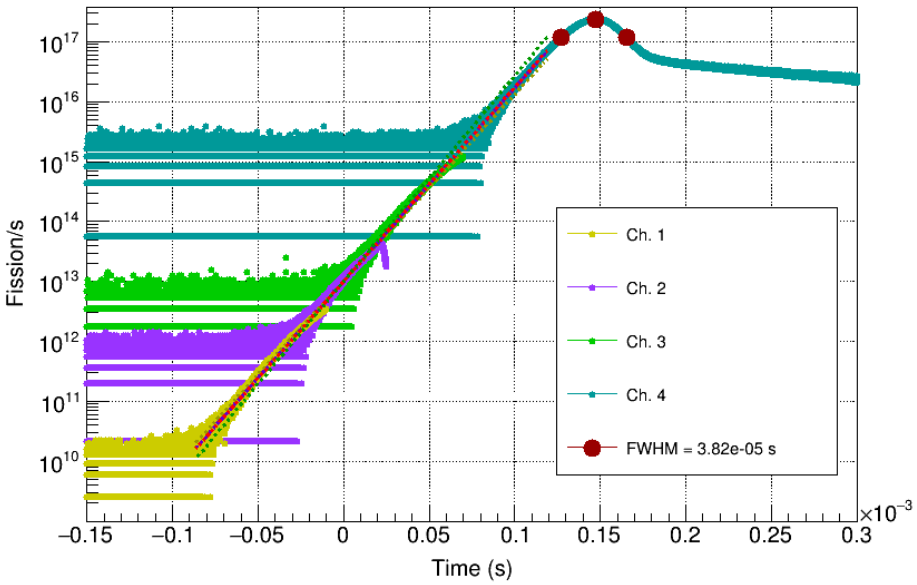

Figure 8: Prompt critical data for the 201°C burst as measured by the 4 channels of the MHD-240. The vertical axis is scaled based on the gamma calibration. The neutron calibration was not considered in this plot. The dashed lines shown are the exponential fit results to each of the channels data.

Table 4: The Godiva temperature, FWHM and alpha for each of the four prompt critical bursts measured by the MHD-240. The attenuation was adjusted on the 168° burst to focus on the low end of the curve and the peak of ch. 4 saturated the scope preventing the determination of the FWHM.

Temp. °C	FWHM (s)	Alpha (generations/μs)
70	2.08 E-4	0.018721
123	6.12 E-5	0.045316
168	–	0.070795
201	3.78 E-5	0.074613

in table 5. The fission yield is dominated by the area under ch. 4, the scaling of ch. 1-3 has little impact on the reported results. However, the assumption of ch. 4 having the correct calibration is a potential source of systematic error. The results in table 5 are broken into three regions; The fit region , the peak region, and the tail region. The fit region covers ch. 1-3 and is the integral exponential fit rather than the integral of the data. This is done since the exact point at which the data goes nonlinear cannot be identified and there are gaps in the overlap of the three channels. The latter two are from ch. 4 data. The split between peak and tail region is identified with the same method used to identify the lower bound of the fit region. It is the point at which the smoothed signal, after the peak, falls below two standard deviations of the RMS baseline noise. An example of how the three regions is split is shown in fig. 10.

5 Conclusion

The first successful PDV measurement of the Godiva-IV assembly was performed and the vibration frequency was measured for two prompt critical bursts. A measurement of the gamma and

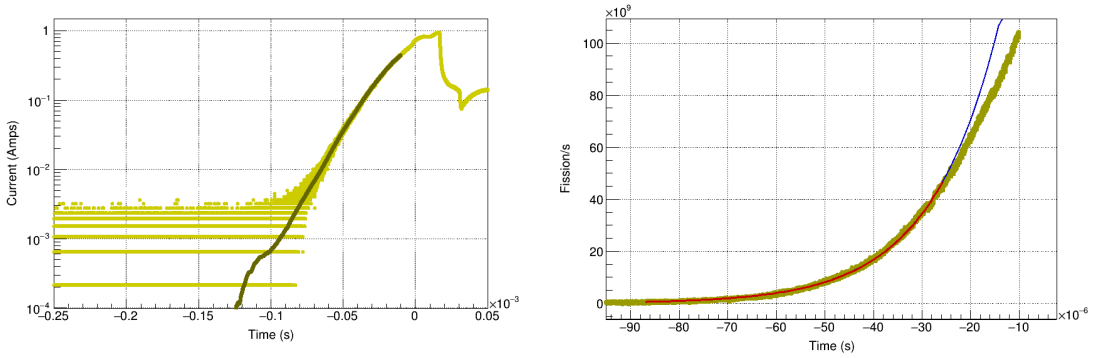

Figure 9: The left plot shows data from ch. 1 with the results of a smoothing algorithm overlaid. The upper bound for the fits search is the point at which the smoothing stops and was identified by eye to be well into the region where the signal is inflecting down, away from exponential rise, and just prior to the erratic saturation behavior, -0.01$\times 10^{-3}$ s. The lower bound was found to be at -0.087$\times 10^{-3}$ s as described in the text. The right plot shows the fit region selected by the search overlaid with the fit results, the red line. The blue line is an extension of the fit to illustrate the deviation from linearity.

Table 5: The integral fission yield in each of the three region and the total. A 4π isotropic correction is assumed. Also shown is the total peak time interval

Temp. °C	Fit	Peak	Peak Time (ms)	Tail	Total
70	3.64×10^{13}	9.74×10^{15}	2.73	1.22×10^{15}	1.10×10^{16}
123	1.17×10^{14}	4.48×10^{16}	0.78	6.45×10^{15}	5.13×10^{16}
201	6.90×10^{13}	5.04×10^{16}	1.69	7.92×10^{15}	5.84×10^{16}

neutron flux of Godiva-IV of four prompt critical bursts were measured with the calibrated MHD-240 detector system. Delayed critical measurements were performed to determine the room return component of the measured Godiva-IV reactivity.

Gamma/neutron calibrations were be used to determine the alpha and total fission yield of the Godiva-IV prompt critical bursts. The analysis reported here used estimates for the leakage gammas and neutrons based on previous calculations to determine the fission yield. An updated MCNP model is in the works to improve our estimates of these values. A room return correction based on the DC measurements has not yet been implemented in the analysis.

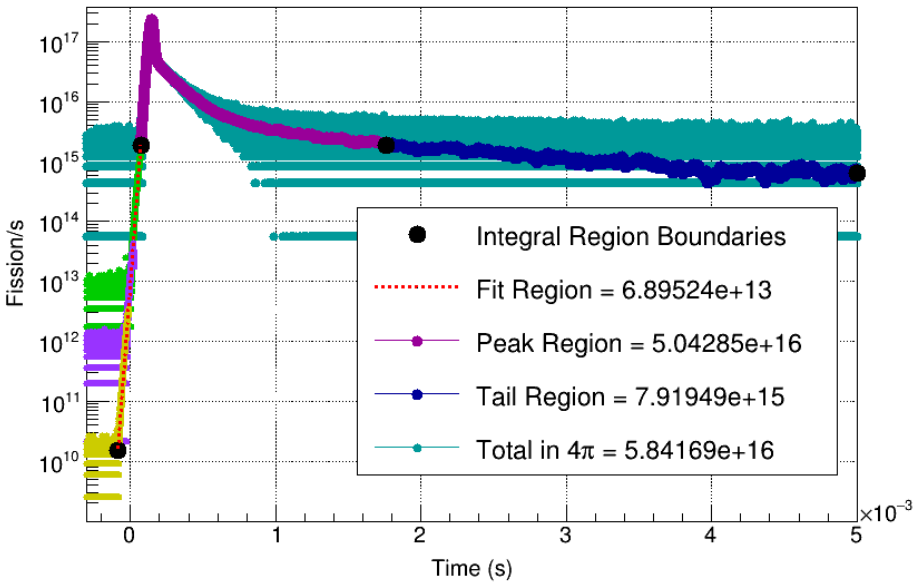

Figure 10: All data for the 201 °C prompt critical burst after conversion to fission/s and the scaling correction to ch. 1-3 are applied. The data is broken into three regions and each is integrated to determine the total fission yield.

Acknowledgments

This work was funded by the United States Department of Energy's Nuclear Criticality Safety Program (NA-511). This work performed under the auspices of the U.S. Department of Energy by Lawrence Livermore National Laboratory under Contract No. DE-AC52-07NA27344. This work was supported by the US Department of Energy through the Los Alamos National Laboratory. Los Alamos National Laboratory is operated by Triad National Security, LLC, for the National Nuclear Security Administration of the US Department of Energy under Contract No. 89233218CNA000001. This work was also supported by Mission Support and Test Services, LLC, under U.S. Department of Energy Contract No. NA0003624.

References

[1] T F Wimett, R H White, and R G Wagner. Godiva iv. Technical Report OSTI-4710389, Los Alamos Scientific Lab, 1970.

[2] R.W. Finlay, C.E. Brient, D.E. Carter, A. Marcinkowski, S. Mellema, G. Randers-Pehrson, and J. Rapaport. The Ohio University beam swinger facility. *Nuclear Instruments and Methods in Physics Research*, 198(2):197 – 206, 1982.

[3] L. Snyder, D. E. Bower, M. J. May, and D. Fittinghoff. Mhd-240 neutron detection efficiency and sensitivity calibration. Technical Report LLNL-TR-807401, Lawrence Livermore National Laboratory, 2020.

[4] Steven Pemberton. Analyzedata v1 software, copyright los alamos national laboratory. Private Communication.

[5] T.F. Wimett, R.H. White, and R.G. Wagner. Godiva IV. *Proceedings of the National Topical Meeting on Fast Burst Reactors, Albuquerque, NM*, pages 95 – 104, 1969.

[6] T. Goorley. Overview of initial Godiva-IV supercritical pulse modeling activities. Technical Report LA-CP-14-00367, Los Alamos National Laboratory.

A Signal Recording System Diagram

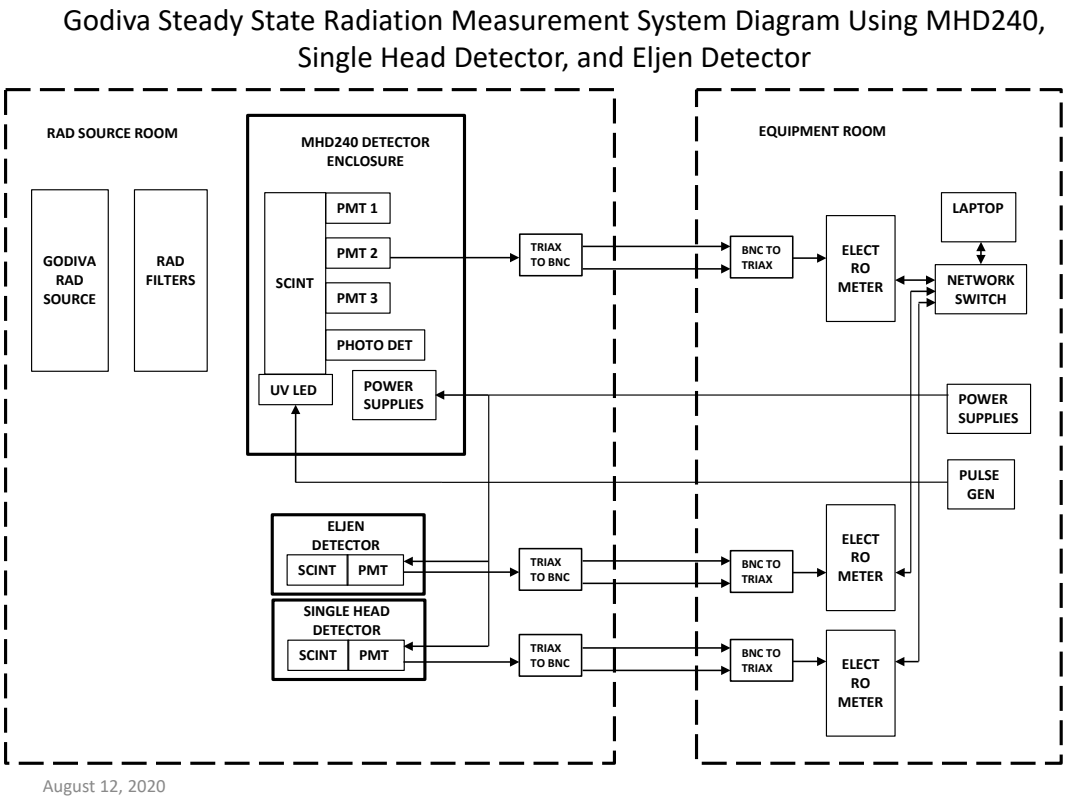

Figure 11: Signal recording diagram for the Delayed Critical measurements

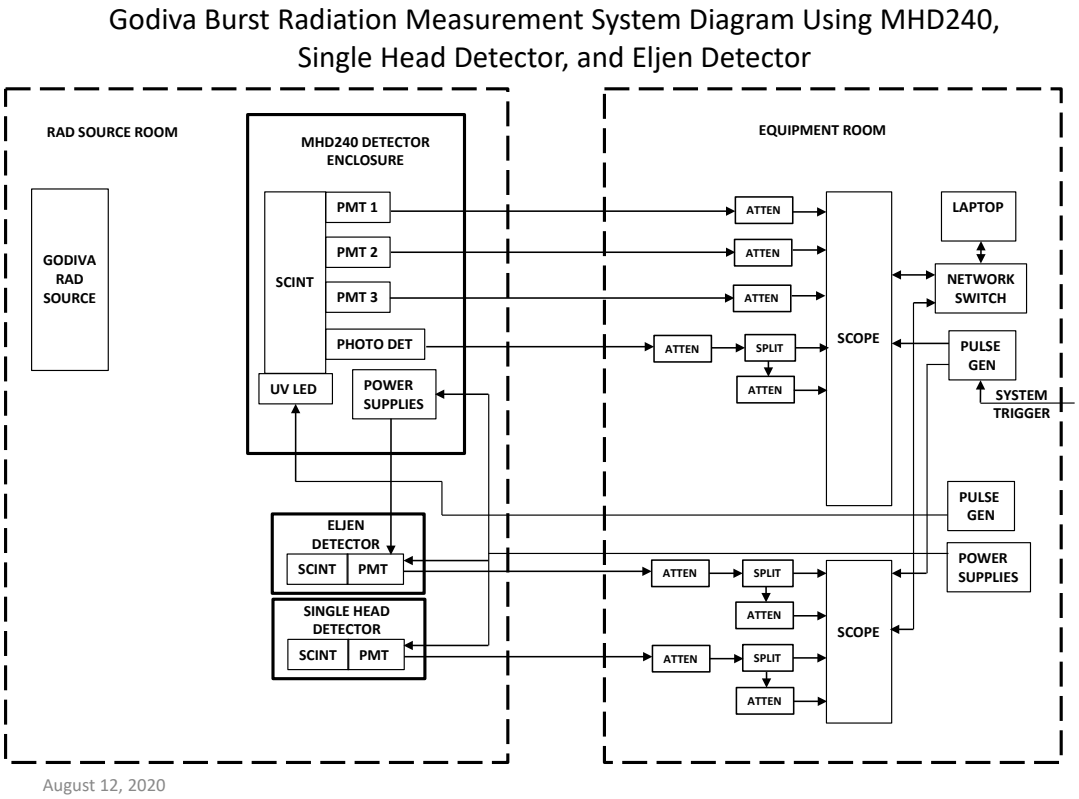

Figure 12: Signal recording diagram for the Prompt Critical measurements. While a split is shown for only the PMT channel in the diagram, in actuality this was done for all four channels. The oscilloscope used was an 8 channel LeCroy HDO8108A.

B Attenuators

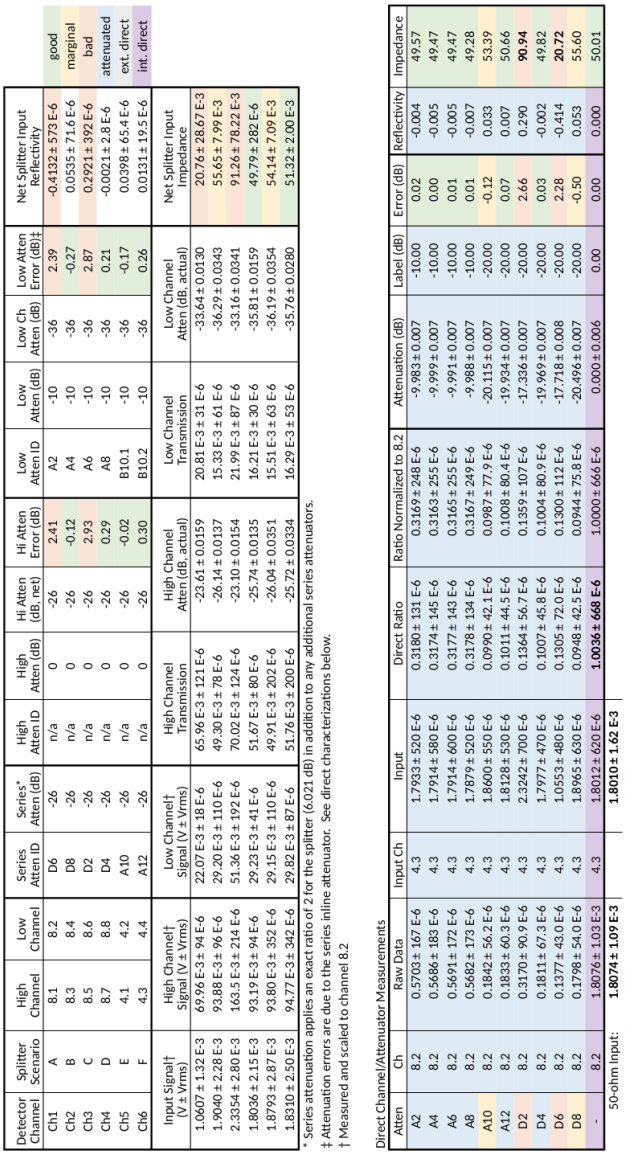

Detector Channel	Splitter Scenario	High Channel	Low Channel	Series Atten ID	Series* Atten (dB)	High Atten ID	High Atten (dB)	Hi Atten (dB, net)	Hi Atten Error (dB)	Low Atten ID	Low Atten (dB)	Low Ch Atten (dB)	Low Atten Error (dB)‡	Net Splitter Input Reflectivity	
Ch1	A	8.1	8.2	D6	-26	n/a	0	-26	2.41	A2	-10	-36	2.39	-0.4132 ± 573 E-6	good
Ch2	B	8.3	8.4	D8	-26	n/a	0	-26	-0.12	A4	-10	-36	-0.27	0.0535 ± 71.6 E-6	marginal
Ch3	C	8.5	8.6	D2	-26	n/a	0	-26	2.93	A6	-10	-36	2.87	0.2921 ± 392 E-6	bad
Ch4	D	8.7	8.8	D4	-26	n/a	0	-26	0.29	A8	-10	-36	0.21	-0.0021 ± 2.8 E-6	attenuated
Ch5	E	4.1	4.2	A10	-26	n/a	0	-26	-0.02	B10.1	-10	-36	-0.17	0.0398 ± 65.4 E-6	ext. direct
Ch6	F	4.3	4.4	A12	-26	n/a	0	-26	0.30	B10.2	-10	-36	0.26	0.0131 ± 19.5 E-6	int. direct

Input Signal† (V ± Vrms)	High Channel† Signal (V ± Vrms)	Low Channel† Signal (V ± Vrms)	High Channel Transmission	Low Channel Transmission	High Channel Atten (dB, actual)	Low Channel Atten (dB, actual)	Net Splitter Input Impedance
1.0607 ± 1.32 E-3	69.96 E-3 ± 94 E-6	22.07 E-3 ± 18 E-6	65.96 E-3 ± 121 E-6	20.81 E-3 ± 31 E-6	-23.61 ± 0.0159	-33.64 ± 0.0130	20.76 ± 28.67 E-3
1.9040 ± 2.28 E-3	93.88 E-3 ± 96 E-6	29.20 E-3 ± 110 E-6	49.30 E-3 ± 78 E-6	15.33 E-3 ± 61 E-6	-26.14 ± 0.0137	-36.29 ± 0.0343	55.65 ± 7.99 E-3
2.3354 ± 2.80 E-3	163.5 E-3 ± 214 E-6	51.36 E-3 ± 192 E-6	70.02 E-3 ± 124 E-6	21.99 E-3 ± 87 E-6	-23.10 ± 0.0154	-33.16 ± 0.0341	91.26 ± 78.22 E-3
1.8036 ± 2.15 E-3	93.19 E-3 ± 94 E-6	29.23 E-3 ± 41 E-6	51.67 E-3 ± 80 E-6	16.21 E-3 ± 30 E-6	-25.74 ± 0.0135	-35.81 ± 0.0159	49.79 ± 282 E-6
1.8793 ± 2.87 E-3	93.80 E-3 ± 352 E-6	29.15 E-3 ± 110 E-6	49.91 E-3 ± 202 E-6	15.51 E-3 ± 63 E-6	-26.04 ± 0.0351	-36.19 ± 0.0354	54.14 ± 7.09 E-3
1.8310 ± 2.50 E-3	94.77 E-3 ± 342 E-6	29.82 E-3 ± 87 E-6	51.76 E-3 ± 200 E-6	16.29 E-3 ± 53 E-6	-25.72 ± 0.0334	-35.76 ± 0.0280	51.32 ± 2.00 E-3

* Series attenuation applies an exact ratio of 2 for the splitter (6.021 dB) in addition to any additional series attenuators.
‡ Attenuation errors are due to the series inline attenuator. See direct characterizations below.
† Measured and scaled to channel 8.2

Direct Channel/Attenuator Measurements

Atten	Ch	Raw Data	Input Ch	Input	Direct Ratio	Ratio Normalized to 8.2	Attenuation (dB)	Label (dB)	Error (dB)	Reflectivity	Impedance
A2	8.2	0.5703 ± 167 E-6	4.3	1.7933 ± 520 E-6	0.3180 ± 131 E-6	0.3169 ± 248 E-6	-9.983 ± 0.007	-10.00	0.02	-0.004	49.57
A4	8.2	0.5686 ± 183 E-6	4.3	1.7914 ± 580 E-6	0.3174 ± 145 E-6	0.3163 ± 255 E-6	-9.999 ± 0.007	-10.00	0.00	-0.005	49.47
A6	8.2	0.5691 ± 172 E-6	4.3	1.7914 ± 600 E-6	0.3177 ± 143 E-6	0.3165 ± 255 E-6	-9.991 ± 0.007	-10.00	0.01	-0.005	49.47
A8	8.2	0.5682 ± 173 E-6	4.3	1.7879 ± 520 E-6	0.3178 ± 134 E-6	0.3167 ± 249 E-6	-9.988 ± 0.007	-10.00	0.01	-0.007	49.28
A10	8.2	0.1842 ± 56.2 E-6	4.3	1.8600 ± 550 E-6	0.0990 ± 42.1 E-6	0.0987 ± 77.9 E-6	-20.115 ± 0.007	-20.00	-0.12	0.033	53.39
A12	8.2	0.1833 ± 60.3 E-6	4.3	1.8128 ± 530 E-6	0.1011 ± 44.5 E-6	0.1008 ± 80.4 E-6	-19.934 ± 0.007	-20.00	0.07	0.007	50.66
D2	8.2	0.3170 ± 90.9 E-6	4.3	2.3242 ± 700 E-6	0.1364 ± 56.7 E-6	0.1359 ± 107 E-6	-17.336 ± 0.007	-20.00	2.66	0.290	**90.94**
D4	8.2	0.1811 ± 67.3 E-6	4.3	1.7977 ± 470 E-6	0.1007 ± 45.8 E-6	0.1004 ± 80.9 E-6	-19.969 ± 0.007	-20.00	0.03	-0.002	49.82
D6	8.2	0.1377 ± 43.0 E-6	4.3	1.0553 ± 480 E-6	0.1305 ± 72.0 E-6	0.1300 ± 112 E-6	-17.718 ± 0.008	-20.00	2.28	-0.414	**20.72**
D8	8.2	0.1798 ± 54.0 E-6	4.3	1.8965 ± 630 E-6	0.0948 ± 42.5 E-6	0.0944 ± 75.8 E-6	-20.496 ± 0.007	-20.00	-0.50	0.053	55.60
-	8.2	1.8076 ± 1.03 E-3	4.3	1.8012 ± 620 E-6	**1.0036 ± 668 E-6**	1.0000 ± 666 E-6	0.000 ± 0.006	0.00	0.00	0.000	50.01
50-ohm input:		**1.8074 ± 1.09 E-3**		**1.8010 ± 1.62 E-3**							
8.2 scaled input				4.3 scaled input							

The last internally terminated channel, and the ratio of 8.2 to 4.3 will be used to baseline all absolute voltage scales, so that reflectivities and impedances of the terminators can be estimated.
This is the most direct test for attenuators, but is very time consuming. Ultimately, we need all attenuators, terminators, and splitters.
We aren't guaranteed an impedance match, nor uniform scaling, so need to mix up the reference channels used.

Figure 13: Attenuation determination for Burst A, 123 ○C

Detector Channel	Splitter Scenario	High Channel	Low Channel	Series Atten ID	Series* Atten (dB)	High Atten ID	High Atten (dB)	Hi Atten (dB, net)	Hi Atten Error (dB)	Low Atten ID	Low Atten (dB)	Low Ch Atten (dB)	Low Atten Error (dB)	Net Splitter Input Reflectivity	
Ch1	A	8.1	8.2	n/a	-6	n/a	0	-6	0.27	B2	-6	-12	-0.05	0.0144 ± 19.2 E-6	good
Ch2	B	8.3	8.4	n/a	-6	n/a	0	-6	0.28	B4	-10	-16	0.05	0.0161 ± 21.4 E-6	marginal
Ch3	C	8.5	8.6	n/a	-6	n/a	0	-6	0.22	B6	-10	-16	0.03	0.0039 ± 5.2 E-6	bad
Ch4	D	8.7	8.8	n/a	-6	n/a	0	-6	0.26	B8	-6	-12	0.01	0.0090 ± 12.0 E-6	attenuated
Ch5	E	4.1	4.2	n/a	-6	B9/C9	-6	-12	-0.06	B10.1	-10	-16	-0.21	0.0093 ± 13.0 E-6	ext. direct
Ch6	F	4.3	4.4	n/a	-6	n/a	0	-6	0.08	n/a	0	-6	0.06	0.0108 ± 15.1 E-6	int. direct

Input Signal† (V ± Vrms)	High Channel† Signal (V ± Vrms)	Low Channel† Signal (V ± Vrms)	High Channel Transmission	High Channel Atten (dB, actual)	Low Channel Transmission	Low Channel Atten (dB, actual)	Net Splitter Input Impedance
1.8334 ± 2.18 E-3	946.1 E-3 ± 1.2 E-3	456.7 E-3 ± 155 E-6	516.0 E-3 ± 915 E-6	-5.747 ± 0.0154	249.1 E-3 ± 309 E-6	-12.073 ± 0.0108	51.46 ± 1.98 E-3
1.8365 ± 2.18 E-3	947.8 E-3 ± 1.0 E-3	292.1 E-3 ± 1.1 E-3	516.1 E-3 ± 828 E-6	-5.745 ± 0.0139	159.0 E-3 ± 624 E-6	-15.970 ± 0.0340	51.64 ± 2.21 E-3
1.8144 ± 2.16 E-3	930.4 E-3 ± 1.4 E-3	288.0 E-3 ± 1.1 E-3	512.8 E-3 ± 985 E-6	-5.801 ± 0.0167	158.7 E-3 ± 622 E-6	-15.987 ± 0.0340	50.39 ± 521 E-6
1.8237 ± 2.18 E-3	939.4 E-3 ± 1.0 E-3	457.7 E-3 ± 606 E-6	515.1 E-3 ± 842 E-6	-5.762 ± 0.0142	251.0 E-3 ± 448 E-6	-12.006 ± 0.0155	50.91 ± 1.23 E-3
1.8242 ± 2.31 E-3	454.1 E-3 ± 1.7 E-3	281.6 E-3 ± 1.1 E-3	248.9 E-3 ± 983 E-6	-12.079 ± 0.0342	154.4 E-3 ± 611 E-6	-16.230 ± 0.0343	50.94 ± 1.33 E-3
1.8269 ± 2.30 E-3	922.1 E-3 ± 1.1 E-3	919.9 E-3 ± 1.1 E-3	504.7 E-3 ± 882 E-6	-5.939 ± 0.0152	503.6 E-3 ± 881 E-6	-5.959 ± 0.0152	51.09 ± 1.54 E-3

* Series attenuation applies an exact ratio of 2 for the splitter (6.021 dB) in addition to any additional series attenuators.

† Measured and scaled to channel 8.2

Direct Channel/Attenuator Measurements

Atten	Ch	Raw Data	Input Ch	Input	Direct Ratio	Ratio Normalized to 8.2	Attenuation (dB)	Label (dB)	Error (dB)	Reflectivity	Impedance
-	8.1	1.8502 ± 1.42 E-3	4.3	1.8508 ± 550 E-6	0.9997 ± 823 E-6	0.9961 ± 1.41 E-3	-0.034 ± 0.012	0	-0.034	0.028	52.84
B2	8.2	0.9321 ± 568 E-6	4.3	1.8549 ± 560 E-6	0.5025 ± 342 E-6	0.5007 ± 671 E-6	-6.008 ± 0.012	-6	-0.008	0.030	53.08
-	8.3	1.9391 ± 757 E-6	4.3	1.9212 ± 660 E-6	1.0093 ± 525 E-6	1.0057 ± 1.27 E-3	0.050 ± 0.011	0	0.050	0.067	57.15
B4	8.4	0.5715 ± 107 E-6	4.3	1.8009 ± 560 E-6	0.3173 ± 115 E-6	0.3162 ± 383 E-6	-10.001 ± 0.011	-10	-0.001	0.000	49.99
-	8.5	1.8469 ± 1.22 E-3	4.3	1.8426 ± 620 E-6	1.0023 ± 743 E-6	0.9988 ± 1.37 E-3	-0.011 ± 0.012	0	-0.011	0.023	52.36
B6	8.6	0.5727 ± 175 E-6	4.3	1.7984 ± 610 E-6	0.3184 ± 145 E-6	0.3173 ± 394 E-6	-9.971 ± 0.011	-10	0.029	-0.001	49.85
-	8.7	1.8639 ± 630 E-6	4.3	1.8553 ± 570 E-6	1.0046 ± 459 E-6	1.0011 ± 1.24 E-3	0.009 ± 0.011	0	0.009	0.030	53.11
B8	8.8	0.9224 ± 647 E-6	4.3	1.8249 ± 550 E-6	0.5054 ± 386 E-6	0.5037 ± 697 E-6	-5.957 ± 0.012	-6	0.043	0.013	51.34
B9/C9	4.1	0.9204 ± 460 E-6	8.1	1.8357 ± 670 E-6	0.5014 ± 310 E-6	0.4993 ± 678 E-6	-6.033 ± 0.012	-6	-0.033	0.019	51.96
B10.1	4.2	0.5578 ± 250 E-6	8.1	1.8107 ± 620 E-6	0.3081 ± 174 E-6	0.3068 ± 409 E-6	-10.263 ± 0.012	-10	-0.263	0.005	50.54
-	4.3	1.8254 ± 485 E-6	8.1	1.8419 ± 1.26 E-3	0.9910 ± 727 E-6	0.9870 ± 1.40 E-3	-0.114 ± 0.012	0	-0.114	0.023	52.32
-	4.4	1.7998 ± 525 E-6	8.1	1.8125 ± 970 E-6	0.9930 ± 605 E-6	0.9889 ± 1.34 E-3	-0.097 ± 0.012	0	-0.097	0.006	50.64

50-ohm Input: **1.8074 ± 1.09 E-3** **1.8010 ± 1.62 E-3** 4.3 Scaled Input

8.2 scaled input **1.8000 ± 2.43 E-3** 8.1 Scaled Input

Channel 8.2 scaling has the best agreement to the average of all measured channels (and is closest to the average impedance of internally terminated, unattenuated channels).
Use 8.2 as the absolute voltage scale reference.

Source input is a fixed constant level, so variances in the input at a channel indicate both reflection and absolute voltage scale variances. These should be separated.

Unattenuated channel ratios should be 1 despite reflections, so variances indicate differences in absolute voltage scale of each channel. These have to all be normalized to a prudent choice.

Odd channels use an external terminator which have a significant mismatch. We cannot use them for impedance references, but can still use them as ratio references for absolute voltage scale.

All impedances should be measured, both attenuated and unattenuated. This provides voltage/current transformation in addition to any voltage attenuation.

Figure 14: Attenuation determination for Burst A, 70 ○C

Detector Channel	Splitter Scenario	High Channel	Low Channel	Series Atten ID	Series* Atten (dB)	High Atten ID	High Atten (dB)	Hi Atten (dB, net)	Hi Atten Error (dB)	Low Atten ID	Low Atten (dB)	Low Ch Atten (dB)	Low Atten Error (dB)	Net Splitter Input Reflectivity	
Ch1	A	8.1	8.2	n/a	-6	n/a	0	-6	0.17	C2	-18	-24	0.30	-0.0046 ± 6.1 E-6	good
Ch2	B	8.3	8.4	n/a	-6	n/a	0	-6	0.27	C4	-15	-21	0.19	0.0152 ± 20.6 E-6	marginal
Ch3	C	8.5	8.6	n/a	-6	n/a	0	-6	0.21	C6	-12	-18	0.03	0.0056 ± 7.5 E-6	bad
Ch4	D	8.7	8.8	n/a	-6	n/a	0	-6	0.25	n/a	0	-6	0.17	0.0068 ± 9.2 E-6	attenuated
Ch5	E	4.1	4.2	n/a	-6	C9/B9	-6	-12	0.02	C10/D10	-20	-26	0.68	0.0182 ± 26.7 E-6	ext. direct
Ch6	F	4.3	4.4	n/a	-6	n/a	0	-6	0.09	n/a	0	-6	0.06	0.0093 ± 14.4 E-6	int. direct

Input Signal† (V ± Vrms)	High Channel† Signal (V ± Vrms)	Low Channel† Signal (V ± Vrms)	High Channel Transmission	High Channel Atten (dB, actual)	Low Channel Transmission	Low Channel Atten (dB, actual)	Net Splitter Input Impedance
1.7992 ± 2.14 E-3	917.5 E-3 ± 1.2 E-3	117.3 E-3 ± 46 E-6	510.0 E-3 ± 917 E-6	-5.849 ± 0.0156	65.17 E-3 ± 82 E-6	-23.719 ± 0.0109	49.55 ± 604 E-6
1.8349 ± 2.23 E-3	945.9 E-3 ± 1.1 E-3	166.7 E-3 ± 623 E-6	515.5 E-3 ± 854 E-6	-5.755 ± 0.0144	90.85 E-3 ± 357 E-6	-20.833 ± 0.0341	51.54 ± 2.13 E-3
1.8175 ± 2.17 E-3	930.9 E-3 ± 1.4 E-3	229.2 E-3 ± 857 E-6	512.2 E-3 ± 997 E-6	-5.812 ± 0.0169	126.1 E-3 ± 495 E-6	-17.986 ± 0.0340	50.56 ± 756 E-6
1.8197 ± 2.20 E-3	936.0 E-3 ± 1.1 E-3	928.4 E-3 ± 1.3 E-3	514.3 E-3 ± 869 E-6	-5.775 ± 0.0147	510.2 E-3 ± 964 E-6	-5.846 ± 0.0164	50.69 ± 934 E-6
1.8403 ± 2.46 E-3	462.4 E-3 ± 1.7 E-3	99.54 E-3 ± 374 E-6	251.3 E-3 ± 996 E-6	-11.997 ± 0.0344	54.09 E-3 ± 216 E-6	-25.338 ± 0.0346	51.85 ± 2.77 E-3
1.8243 ± 2.58 E-3	922.1 E-3 ± 1.1 E-3	918.8 E-3 ± 1.1 E-3	505.5 E-3 ± 942 E-6	-5.926 ± 0.0162	503.7 E-3 ± 941 E-6	-5.957 ± 0.0162	50.94 ± 1.46 E-3

* Series attenuation applies an exact ratio of 2 for the splitter (6.021 dB) in addition to any additional series attenuators.

† Measured and scaled to channel 8.2

Direct Channel/Attenuator Measurements

Atten	Ch	Raw Data	Input Ch	Input	Direct Ratio Ch/Input	Ratio Normalized to 8.2	Attenuation (dB)	Label (dB)	Error (dB)	Reflectivity	Impedance
-	8.1	1.8500 ± 896 E-6	4.3	1.8515 ± 598 E-6	0.9992 ± 582 E-6	0.9957 ± 1.29 E-3	-0.038 ± 0.011	0	-0.038	0.0280	52.88
C2	8.2	0.2250 ± 77.0 E-6	4.3	1.7449 ± 690 E-6	0.1289 ± 67.4 E-6	0.1285 ± 163 E-6	-17.824 ± 0.011	-18	0.176	-0.0312	46.98
-	8.3	1.9392 ± 660 E-6	4.3	1.9228 ± 610 E-6	1.0085 ± 469 E-6	1.0050 ± 1.25 E-3	0.043 ± 0.011	0	0.043	0.0676	57.25
C4	8.4	0.3186 ± 127 E-6	4.3	1.7902 ± 540 E-6	0.1779 ± 89.0 E-6	0.1773 ± 223 E-6	-15.025 ± 0.011	-15	-0.025	-0.0060	49.40
-	8.5	1.8465 ± 1.28 E-3	4.3	1.8441 ± 530 E-6	1.0013 ± 751 E-6	0.9978 ± 1.37 E-3	-0.020 ± 0.012	0	-0.020	0.0239	52.45
C6	8.6	0.4539 ± 176 E-6	4.3	1.8047 ± 520 E-6	0.2515 ± 122 E-6	0.2506 ± 314 E-6	-12.019 ± 0.011	-12	-0.019	0.0020	50.20
-	8.7	1.8644 ± 644 E-6	4.3	1.8572 ± 490 E-6	1.0039 ± 436 E-6	1.0003 ± 1.23 E-3	0.003 ± 0.011	0	0.003	0.0312	53.22
-	8.8	1.8043 ± 775 E-6	4.3	1.8034 ± 600 E-6	**1.0005 ± 544 E-6**	0.9970 ± 1.27 E-3	-0.026 ± 0.011	0	-0.026	0.0013	50.13
C9	4.1	0.9203 ± 460 E-6	8.1	1.8303 ± 1.45 E-3	0.5028 ± 471 E-6	0.5007 ± 765 E-6	-6.008 ± 0.013	-6	-0.008	0.0168	51.71
C10/D10	4.2	0.1983 ± 64.3 E-6	8.1	1.8773 ± 1.25 E-3	0.1056 ± 78.2 E-6	0.1052 ± 149 E-6	-19.560 ± 0.012	-20	0.440	0.0429	54.49
-	4.3	1.8255 ± 503 E-6	8.1	1.8385 ± 1.30 E-3	**0.9929 ± 754 E-6**	0.9889 ± 1.41 E-3	-0.097 ± 0.012	0	-0.097	0.0214	52.19
-	4.4	1.8004 ± 670 E-6	8.1	1.8102 ± 1.32 E-3	**0.9946 ± 814 E-6**	0.9905 ± 1.45 E-3	-0.083 ± 0.013	0	-0.083	0.0057	50.57
50-ohm Input:		**1.8074 ± 1.09 E-3**		**1.8010 ± 1.62 E-3**	4.3 Scaled Input						
8.2 scaled input				**1.8000 ± 2.43 E-3**	8.1 Scaled Input						

Input is a fixed constant level, so variances in the input (for a given input channel) are due to reflections from the probed channel/attenuator.
Ratios of unattenuated channels should be 1 despite any reflections, so variances indicate relative absolute voltage scaling between channels.
Odd channels use an external terminator and have a mismatch. Once absolute reference is normalized, then we can calculate reflections from the external terminators and/or attenuators.
The only internally-terminated, even channels are 8.2, 8.8, and 4.4. First, scale them all to 8.2 and then use their average to represent the matched condition with no reflection.
Channels 8.8 and 4.4 are internally terminated and have good match. But 8.2 is slightly better, as both a voltage reference, and 50 ohms.

Figure 15: Attenuation determination for Burst C, 168 ○C

Detector Channel	Splitter Scenario	High Channel	Low Channel	Series Atten ID	Series* Atten (dB)	High Atten ID	High Atten (dB)	Hi Atten (dB, net)	Hi Atten Error (dB)	Low Atten ID	Low Atten (dB)	Low Ch Atten (dB)	Low Atten Error (dB)	Net Splitter Input Reflectivity	
Ch1	A	8.1	8.2	n/a	-6	D1	-3	-9	0.55	D2	-20	-26	3.82	0.0934 ± 125 E-6	good
Ch2	B	8.3	8.4	n/a	-6	D3	-3	-9	0.34	D4	-20	-26	0.21	0.0143 ± 19.1 E-6	marginal
Ch3	C	8.5	8.6	n/a	-6	D5	-3	-9	-0.71	D6	-20	-26	0.03	-0.1084 ± 152 E-6	bad
Ch4	D	8.7	8.8	n/a	-6	D7	-9	-15	0.17	D8	-20	-26	-0.14	0.0126 ± 16.9 E-6	attenuated
Ch5	E	4.1	4.2	n/a	-6	D9	-3	-9	0.09	D10/C10	-20	-26	0.67	0.0153 ± 22.7 E-6	ext. direct
Ch6	F	4.3	4.4	n/a	-6	n/a	0	-6	0.10	D12	0	-6	0.05	0.0097 ± 15.5 E-6	int. direct

Input Signal† (V ± Vrms)	High Channel† Signal (V ± Vrms)	Low Channel† Signal (V ± Vrms)	High Channel Transmission	High Channel Atten (dB, actual)	Low Channel Transmission	Low Channel Atten (dB, actual)	Net Splitter Input Impedance (ohms)
1.9761 ± 2.37 E-3	0.7453 ± 1.0 E-3	0.1534 ± 349 E-6	377.1 E-3 ± 685 E-6	-8.470 ± 0.0158	77.61 E-3 ± 200 E-6	-22.202 ± 0.0223	60.30 ± 15.3 E-3
1.8333 ± 2.18 E-3	0.6751 ± 774 E-6	0.0939 ± 351 E-6	368.3 E-3 ± 609 E-6	-8.677 ± 0.0144	51.20 E-3 ± 201 E-6	-25.814 ± 0.0340	51.45 ± 1.97 E-3
1.6116 ± 2.03 E-3	0.5258 ± 688 E-6	0.0809 ± 302 E-6	326.3 E-3 ± 593 E-6	-9.728 ± 0.0158	50.17 E-3 ± 198 E-6	-25.991 ± 0.0342	40.22 ± 12.3 E-3
1.8302 ± 2.19 E-3	0.3312 ± 336 E-6	0.0900 ± 119 E-6	181.0 E-3 ± 284 E-6	-14.848 ± 0.0136	49.19 E-3 ± 88 E-6	-26.163 ± 0.0155	51.28 ± 1.73 E-3
1.8350 ± 2.49 E-3	0.6563 ± 2.5 E-3	0.0991 ± 373 E-6	357.6 E-3 ± 1.4 E-3	-8.931 ± 0.0347	54.02 E-3 ± 216 E-6	-25.349 ± 0.0347	51.55 ± 2.34 E-3
1.8250 ± 2.68 E-3	0.9226 ± 1.1 E-3	0.9178 ± 1.1 E-3	505.5 E-3 ± 964 E-6	-5.925 ± 0.0165	502.9 E-3 ± 959 E-6	-5.971 ± 0.0165	50.98 ± 1.58 E-3

* Series attenuation applies an exact ratio of 2 for the splitter (6.021 dB) in addition to any additional series attenuators.

† Measured, unscaled by attenuator settings, and scaled to channel 8.2

Direct Attenuator Measurements

Atten	Atten Ch	Raw Data	Unscaled Data	Input Ch	Input	Unscaled Input	Direct Ratio	Ratio Normalized to 8.2	Attenuation (dB)	Label	dB error	Reflectivity	Impedance
D1	8.1	3.7779 ± 1.80 E-3	1.3373 ± 637 E-6	4.3	3.7449 ± 1.41 E-3	1.8725 ± 705 E-6	0.7142 ± 434 E-6	0.7117 ± 928 E-6	-2.95 ± 0.011	-3.00	0.05	0.0397	54.13
D2	8.2	6.3381 ± 2.44 E-3	0.3169 ± 122 E-6	4.3	4.6469 ± 1.54 E-3	2.3235 ± 770 E-6	0.1364 ± 69.3 E-6	0.1359 ± 171 E-6	-17.33 ± 0.011	-20.00	2.67	0.2901	**90.86**
D3	8.3	3.9041 ± 1.67 E-3	1.3819 ± 591 E-6	4.3	3.8196 ± 1.15 E-3	1.9098 ± 575 E-6	0.7236 ± 379 E-6	0.7210 ± 914 E-6	-2.84 ± 0.011	-3.00	0.16	0.0604	56.43
D4	8.4	3.6241 ± 1.51 E-3	0.1812 ± 75.5 E-6	4.3	3.6048 ± 1.13 E-3	1.8024 ± 565 E-6	0.1005 ± 52.4 E-6	0.1002 ± 127 E-6	-19.98 ± 0.011	-20.00	0.02	0.0008	50.08
D5	8.5	3.7118 ± 2.18 E-3	1.3139 ± 772 E-6	4.3	3.6407 ± 1.08 E-3	1.8204 ± 540 E-6	0.7218 ± 475 E-6	0.7192 ± 955 E-6	-2.86 ± 0.012	-3.00	0.14	0.0107	51.08
D6	8.6	2.7485 ± 860 E-6	0.1374 ± 43.0 E-6	4.3	2.1302 ± 770 E-6	1.0651 ± 385 E-6	0.1290 ± 61.7 E-6	0.1286 ± 161 E-6	-17.82 ± 0.011	-20.00	2.18	-0.4086	**20.99**
D7	8.7	3.7434 ± 3.00 E-3	0.6641 ± 532 E-6	4.3	3.5880 ± 1.11 E-3	1.7940 ± 555 E-6	0.3702 ± 318 E-6	0.3689 ± 531 E-6	-8.66 ± 0.012	-9.00	0.34	-0.0039	49.61
D8	8.8	3.5921 ± 1.55 E-3	0.1796 ± 77.5 E-6	4.3	3.7968 ± 1.39 E-3	1.8984 ± 695 E-6	0.0946 ± 53.5 E-6	0.0943 ± 121 E-6	-20.51 ± 0.011	-20.00	-0.51	0.0541	55.72
D9	4.1	3.6445 ± 1.54 E-3	1.2901 ± 545 E-6	8.1	5.1202 ± 2.75 E-3	1.8124 ± 973 E-6	0.7118 ± 486 E-6	0.7145 ± 832 E-6	-2.92 ± 0.010	-3.00	0.08	0.0069	50.69
D10	4.2	3.9691 ± 1.34 E-3	0.1985 ± 67.0 E-6	8.1	5.3062 ± 3.94 E-3	1.8783 ± 1.39 E-3	0.1057 ± 86.2 E-6	0.1061 ± 132 E-6	-19.49 ± 0.011	-20.00	0.51	0.0435	54.54
-	4.3	3.6496 ± 1.07 E-3	1.8248 ± 535 E-6	8.1	5.1849 ± 1.89 E-3	1.8353 ± 669 E-6	0.9943 ± 465 E-6	0.9980 ± 1.05 E-3	-0.02 ± 0.009	0.00	-0.02	0.0196	52.00
-	4.4	3.5997 ± 1.13 E-3	1.7999 ± 565 E-6	8.1	5.1194 ± 2.40 E-3	1.8121 ± 850 E-6	0.9932 ± 560 E-6	0.9969 ± 1.09 E-3	-0.03 ± 0.010	0.00	-0.03	0.0067	50.68
		50-ohm Input:	**1.8074 ± 1.09 E-3**			**1.8010 ± 1.62 E-3**	4.3 Scaled Input						
		8.2 scaled input				**1.8000 ± 2.43 E-3**	8.1 Scaled Input						

Figure 16: Attenuation determination for Burst D, 201 ○C

Scope Channels	Relat ve Channel Sensit vit es		At enuator Errors Burst A (dB)	At enuator Errors Burst B (dB)	At enuator Errors Burst C (dB)	At enuator Errors Burst D (dB)
Ch 8.1	0.9959 ± 0.001		2.406 ± 0.016	0.274 ± 0.015	0.171 ± 0.016	0.550 ± 0.016
Ch 8.3	1.0054 ± 0.001		-0.122 ± 0.014	0.275 ± 0.014	0.266 ± 0.014	0.344 ± 0.014
Ch 8.5	0.9983 ± 0.001		2.925 ± 0.015	0.219 ± 0.017	0.209 ± 0.017	-0.708 ± 0.016
Ch 8.7	1.0007 ± 0.001		0.285 ± 0.014	0.259 ± 0.014	0.245 ± 0.015	0.173 ± 0.014
Ch 4.1	1.0006 ± 0.004		-0.016 ± 0.035	-0.058 ± 0.034	0.023 ± 0.034	0.090 ± 0.035
Ch 4.3	0.9965 ± 0.001		0.300 ± 0.033	0.082 ± 0.015	0.095 ± 0.016	0.095 ± 0.017
Ch 8.2	1.0000 ± 0.000		2.386 ± 0.013	-0.052 ± 0.013	0.301 ± 0.011	3.819 ± 0.022
Ch 8.4	1.0015 ± 0.004		-0.266 ± 0.034	0.051 ± 0.034	0.187 ± 0.034	0.206 ± 0.034
Ch 8.6	1.0015 ± 0.004		2.865 ± 0.034	0.033 ± 0.034	0.035 ± 0.034	0.030 ± 0.034
Ch 8.8	0.9970 ± 0.001		0.214 ± 0.016	0.014 ± 0.016	0.175 ± 0.016	-0.142 ± 0.016
Ch 4.2	1.0006 ± 0.004		-0.167 ± 0.035	-0.209 ± 0.035	0.683 ± 0.035	0.671 ± 0.035
Ch 4.4	0.9973 ± 0.001		0.258 ± 0.028	0.062 ± 0.028	0.063 ± 0.016	0.050 ± 0.017
Detector Channels	**High Channel**	**Low Channel**	**Input Impedance Burst A (ohms)**	**Input Impedance Burst B (ohms)**	**Input Impedance Burst C (ohms)**	**Input Impedance Burst D (ohms)**
Ch 1	Ch 8.1	Ch 8.2	20.763 ± 0.029	51.458 ± 0.002	49.545 ± 0.001	60.296 ± 0.015
Ch 2	Ch 8.3	Ch 8.4	55.648 ± 0.008	51.635 ± 0.002	51.544 ± 0.002	51.452 ± 0.002
Ch 3	Ch 8.5	Ch 8.6	91.263 ± 0.078	50.389 ± 0.001	50.563 ± 0.001	40.223 ± 0.012
Ch 4	Ch 8.7	Ch 8.8	49.788 ± 0.000	50.906 ± 0.001	50.686 ± 0.001	51.275 ± 0.002
Ch 5	Ch 4.1	Ch 4.2	54.142 ± 0.007	50.936 ± 0.001	51.850 ± 0.003	51.551 ± 0.002
Ch 6	Ch 4.3	Ch 4.4	51.323 ± 0.002	51.089 ± 0.002	50.942 ± 0.001	50.982 ± 0.002

Figure 17: Attenuation determination and impedance measurement summarized for all four prompt critical bursts.

C Gamma Sensitivity

Calibration Data Sheet Remarks Section

Detector:	MHD-240-4	Serial No.:	016	Drawing No:	#N/A	Calibration Date:	14-Jan-13	National Security Technologies LLC Vision • Service • Partnership		
Detector Head	PMH-350	Head S/N:	43	Calibrated Operating Voltage	-2242	Radiation Sensitivity	C/y-MeV	4.51E-12	Maximum Operating Voltage	-2500
REMARKS										
Detector Head	PMH-350	Head S/N:	044	Calibrated Operating Voltage	-1170	Radiation Sensitivity	C/y-MeV	4.53E-14	Maximum Operating Voltage	-2500
REMARKS										
Detector Head	PMH-350	Head S/N:	45	Calibrated Operating Voltage	-1785	Radiation Sensitivity	C/y-MeV	4.50E-16	Maximum Operating Voltage	-2500
REMARKS										
Detector Head	PDH-4	Head S/N:	1013LV	Calibrated Operating Voltage	1000	Radiation Sensitivity	C/y-MeV	2.12E-18	Maximum Operating Voltage	8000
REMARKS										
S-4, 1/4"GAP, 37%										
Calibration By	Irene Garza	Date	14-Jan-13	Approved BY	Brent Davis			Date	17-Jan-13	

Figure 18: Gamma sensitivity calibrations data sheet.

Detector:	MHD-240-4		Serial No.:	016	Drawing No:	#N/A		Fluor Type:	6"CUBE BC-404	Detector Characterization Data Sheet				Calibration Date:	14-Jan-13	National Security Technologies LLC		
Detector Head	Max. Linear Output (volts)	Phototube Noise Floor @ 250 MHz (Volts)	Quality Factor 250 MHz (dB)	Transit Time [30% amplitude (ns)]	Signal Impulse FWHM (ns)	Signal Impulse Rise Time (ns)	Signal Step Rise Time (ns)	PMT Gain	Radiation Source ID	Calibration Distance	Collimator Diameter		Radiation Intensity	Calibration Voltage (Volts)	Dark Current @ Calibration Voltage (Amps)	Radiated Current (Amps)	Sensitivity Adjustment Factor	Radiation Sensitivity
										See W2			γ-MeV/sec					C/γ-MeV
PMH-350-43														-3000				
														-2900				
Optical Filter														-2800				
NONE														-2700				
														-2600				
Remarks	33.00	1.560	26.51	5.792	2.61	1.43	3.08							-2500				
														-2400				
														-2300				
														-2200				
														-2100				
	26.00	0.322	38.14	6.267	2.94	1.63	3.38							-2000				
														-1900				
														-1800				
														-1700				
														-1600				
	20.00	0.039	54.20	7.055	3.41	1.91	3.85							-1500				
														-1400				
														-1300				
														-1200				
	14.00	0.005	68.943	8.254	4.34	2.521	4.95							-1100				
Operating Voltage									SR3-92	30.00	4	in	2.88E+04	-2242	5.00E-09	1.35E-07	1	4.51E-12

Detector Head	Signal Max. Linear Output (volts)	Phototube Noise Floor @ 250 MHz (Volts)	Quality Factor 250 MHz (dB)	Transit Time 30% amplitude (ns)	Signal Impulse FWHM (ns)	Signal Impulse Rise Time (ns)	Signal Step Rise Time (ns)	PMT Gain	Radiation Source ID	Calibration Distance	Collimator Diameter		Radiation Intensity	Calibration Voltage (Volts)	Dark Current @ Calibration Voltage (Amps)	Radiated Current (Amps)	Sensitivity Adjustment Factor	Radiation Sensitivity
										See Y2			γ-MeV/sec					C/γ-MeV
PMH-350-044														-3000				
														-2900				
Optical Filter														-2800				
NONE														-2700				
														-2600				
Remarks	30.00	2.200	22.694	5.908	2.739	1.502	2.633							-2500				
														-2400				
														-2300				
														-2200				
														-2100				
	25.00	0.422	35.453	6.511	2.997	1.701	2.883							-2000				
														-1900				
														-1800				
														-1700				
														-1600				
	18.00	0.041	52.850	7.313	3.373	2.026	3.382							-1500				
														-1400				
														-1300				
														-1200				
	13.00	0.005	68.299	8.657	4.019	2.614	4.306							-1100				
Operating Voltage									SR3-92	30.00	4	in	2.88E+04	-1170	4.50E-11	1.35E-09	1	4.53E-14

Calibration By	Irene Garza	Date:	14-Jan-13	Approved by:	Brent Davis	Approval Date	17-Jan-13

Figure 19: Gamma sensitivity calibrations data sheet.

Detector Head	Signal Max. Linear Output (volts)	Phototube Noise Floor @ 250 MHz (Volts)	Quality Factor 250 MHz (dB)	Transit Time 30% amplitude (ns)	Signal Impulse FWHM (ns)	Signal Impulse Rise Time (ns)	Signal Step Rise Time (ns)	PMT Gain	Radiation Source ID	Calibration Distance	Collimator Diameter		Radiation Intensity	Calibration Voltage (Volts)	Dark Current @ Calibration Voltage (Amps)	Radiated Current (Amps)	Sensitivity Adjustment Factor	Radiation Sensitivity
										See AA2			γ-MeV/sec					C/γ-MeV
PMH-350-45														-3000				
														-2900				
Optical Filter														-2800				
														-2700				
ND 3.0														-2600				
Remarks	31.00	2.700	21.200	5.554	2.563	1.393	3.009							-2500				
														-2400				
														-2300				
														-2200				
														-2100				
	25.00	0.618	32.139	6.156	2.864	1.571	3.304							-2000				
														-1900				
														-1800				
														-1700				
														-1600				
	20.00	0.075	48.519	6.881	3.338	1.867	3.763							-1500				
														-1400				
														-1300				
														-1200				
	14.00	0.005	68.943	7.925	4.252	2.417	4.892							-1100				
Operating Voltage									SR2-2	100.00	4	in	1.22E+09	**-1785**	6.00E-10	5.50E-07	1	4.50E-16

Detector Head	Signal Max. Linear Output (volts)	Phototube Noise Floor @ 250 MHz (Volts)	Quality Factor 250 MHz (dB)	Transit Time 30% amplitude (ns)	Signal Impulse FWHM (ns)	Signal Impulse Rise Time (ns)	Signal Step Rise Time (ns)	PMT Gain	Radiation Source ID	Calibration Distance	Collimator Diameter		Radiation Intensity	Calibration Voltage (Volts)	Dark Current @ Calibration Voltage (Amps)	Radiated Current (Amps)	Sensitivity Adjustment Factor	Radiation Sensitivity
										See AC2			γ-MeV/sec					C/γ-MeV
PDH-4-1013LV														-3000				
														-2900				
Optical Filter														-2800				
Not Specified														-2700				
														-2600				
Remarks														-2500				
														-2400				
														-2300				
														-2200				
														-2100				
														-2000				
														-1900				
														-1800				
														-1700				
														-1600				
														-1500				
														-1400				
														-1300				
														-1200				
														-1100				
Operating Voltage									SR2-1	100.00	4	in	3.07E+10	**1000**	4.20E-12	6.50E-08	1	2.12E-18

Page 2 of 2	Calibration By:	Irene Garza	Date:	14-Jan-13	Approved by:	Brent Davis	Approval Date:	17-Jan-13

Figure 20: Gamma sensitivity calibrations data sheet.

D Recorded Burst Data

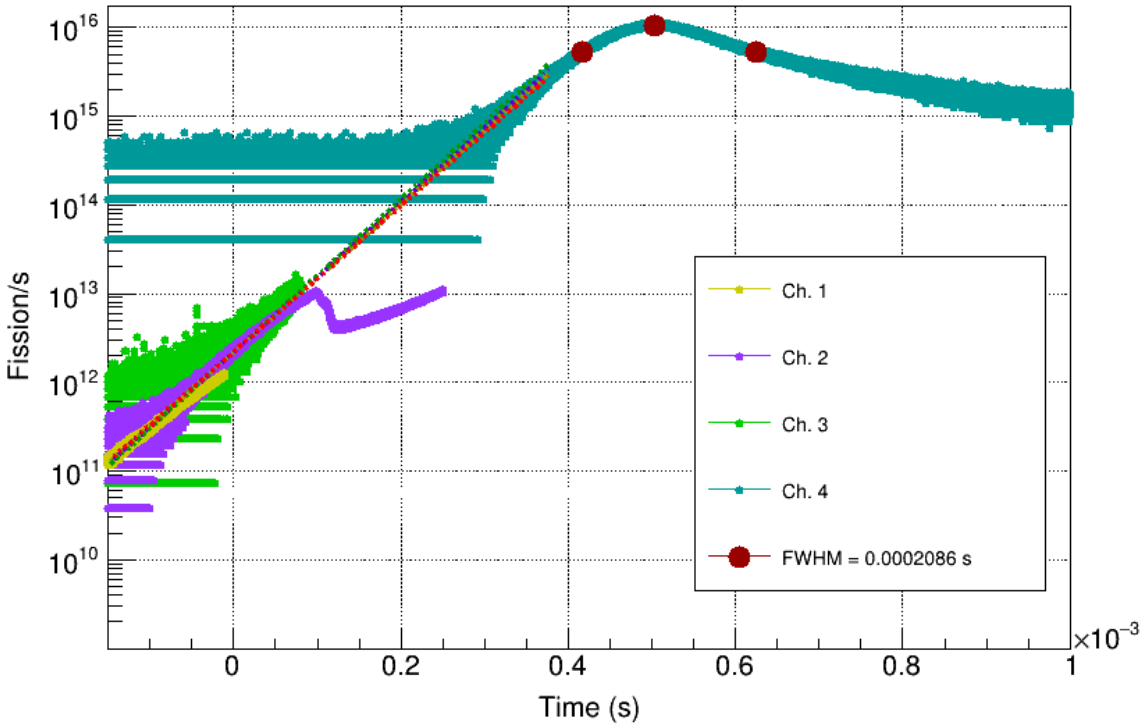

Figure 21: The 70 °C burst.

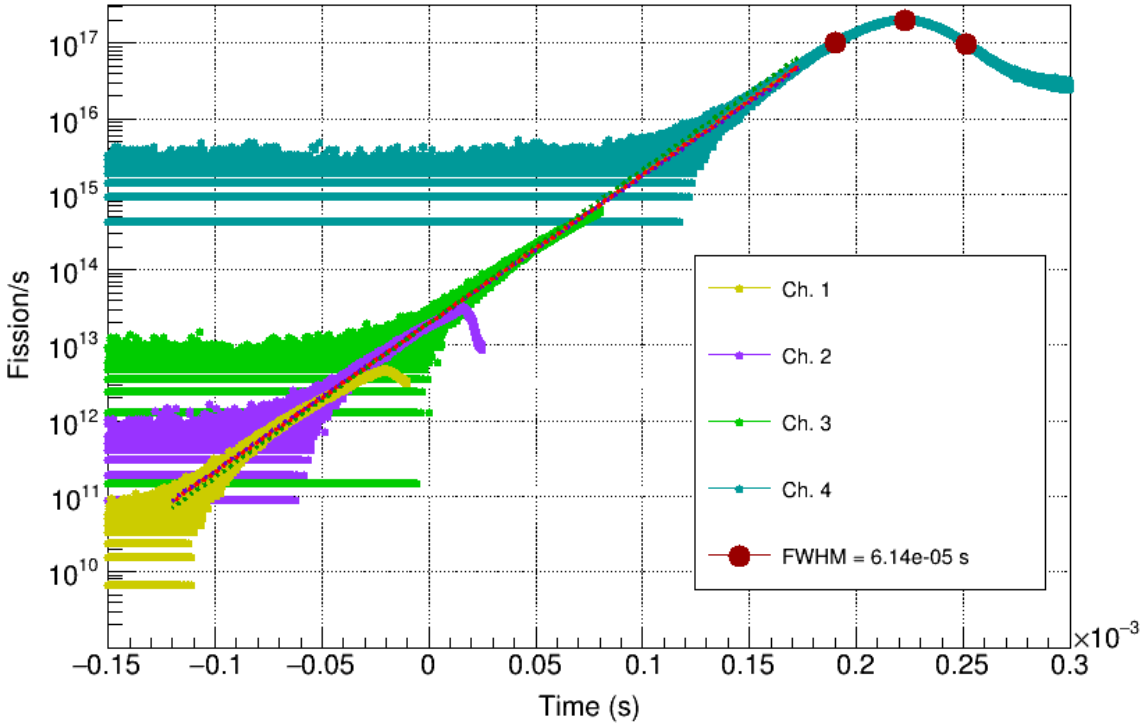

Figure 22: The 123 °C burst.

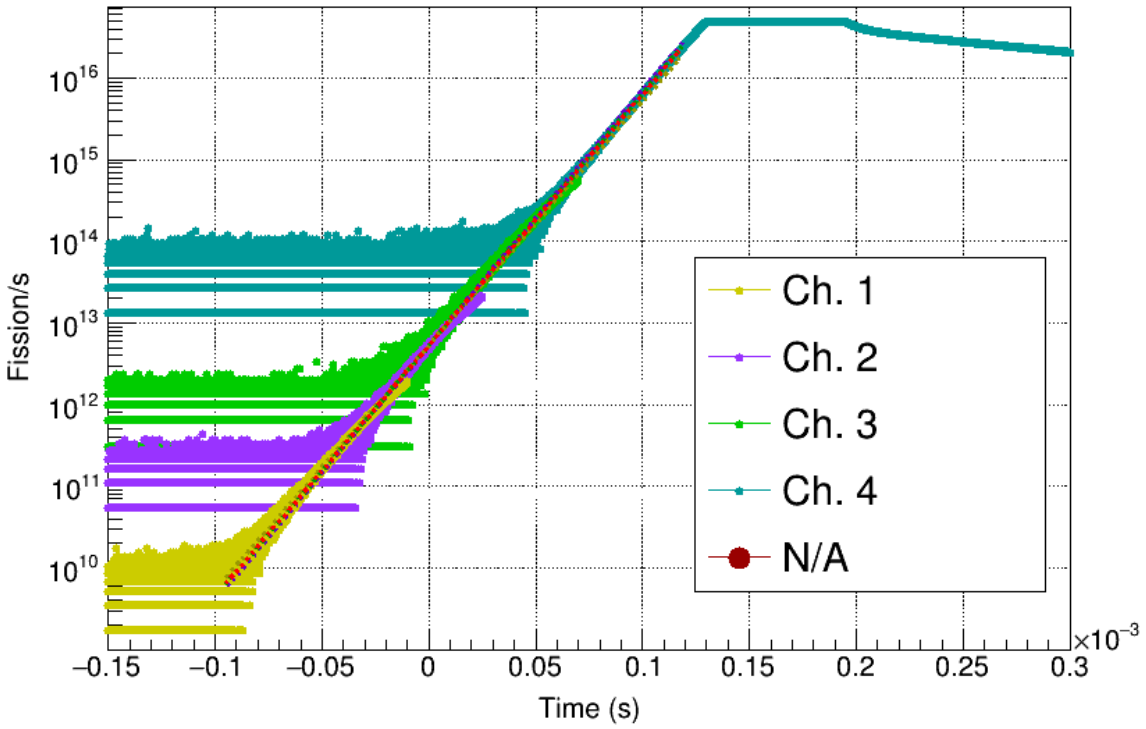

Figure 23: The 168 °C burst.